ELSEVIER

Journal of Chromatography A, 759 (1997) 27–35

JOURNAL OF CHROMATOGRAPHY A

Surface plasmon resonance-based detection An alternative to refractive index detection in high-performance liquid chromatography

G. Cepria, J.R. Castillo*

G.E.A.S. (Group of Analytical Spectroscopy and Sensors), Department of Analytical Chemistry, Faculty of Sciences, University of Zaragoza, Campus Plaza San Francisco, 50009 Zaragoza, Spain

Received 18 March 1996; revised 28 August 1996; accepted 29 August 1996

Abstract

The surface plasmon resonance (SPR) effect was exploited to develop a detector responding to changes in the refractive index for use in high-performance liquid chromatography. The performance of the SPR detector was compared with that of a refractive index (RI) detector from Hewlett-Packard. The effects of the optical fibre connections and light-emitting diode wavelengths (1300 and 850 nm) were studied. The detectors that were tested provided similar limits of detection for the sugars, fructose (7 μg for RI and 5 μg for SPR), glucose (7 μg for RI and 13 μg for SPR) and sucrose (13 μg for RI and 22 μg for SPR). The SPR was found to reach a stable baseline quicker than the RI detector, i.e., 50 min before the RI detector did.

Keywords: Surface plasmon resonance detection; Refractive index detection; Detection, LC; Sugars

1. Introduction

Detectors based on changes in the refractive index (RI) are widely used since they are non-specific. Although RI is a universal property, the differences in the absolute values for substances are small, which constitutes a great drawback, since the sensitivity achieved is moderate. Indeed, the RI is very sensitive to small changes in temperature and pressure. The temperature must be kept constant, within an interval of ±0.001°C in order to reach the highest sensitivity available, i.e. 10^{-6} RI units.

Several new designs have been reported [1] with which higher sensitivity can be reached but they are complicated and some of them, like refractometers, are quite expensive.

RI detectors are based on three phenomena, namely refraction, reflection and interference. But there is another parameter that is also related to changes in RI, that is, surface plasmon resonance (SPR).

A surface plasmon is a charge density wave propagating along a metal–dielectric surface [2]. Such a two-phase system can be analyzed using the Maxwell equation.

$$Ksp = w/c\sqrt{(e_1 e_2/(e_1 + e_2))}$$

Where Ksp is the wave vector for the plasmon, e_1 is the real part of the dielectric constant of the metal at frequency, w, e_2 is the real part of the dielectric

*Corresponding author.

PII S0021-9673(96)00752-2

constant of the dielectric medium and c is the speed of light.

This phenomenon takes place when $|e_1| < -e_2$. This condition is satisfied by most metals interfacing with air or some ligand, at visible and near-infrared wavelengths.

The resulting wave can be coupled to p-polarized light to produce the SPR effect, which only takes place at a given light incidence angle onto the metal surface and depends on the nature of the metal and dielectric concerned, as well as the wavelength. For monochromatic light, the excitation of a surface plasmon is manifested by a sharp minimum in the reflectance when the angle of incidence is varied. The narrowest resonance is produced by material whose dielectric constants have the highest real-to-imaginary part of the dielectric constant ratio, which corresponds to silver (37.96), copper (20.38), gold (7.33) and aluminium (2.56). This is why these metals are the most widely used to design SPR sensors [19]. Among them, gold is the most generally used due to its chemical stability.

Once the resonance is achieved, the molecules entering or leaving the plasmon field induce local changes in the RI, which is directly related to the dielectric constant: $e = n^2$. This change produces a variation in the resonance peak, as a consequence, the intensity of the emerging light varies in a way that is proportional to the difference in the RI.

Essentially, the SPR effect has so far been used to design optical sensors for specific detection in biosensing and immunoassays. For this purpose, a ligand, interacting biospecifically with a biomolecule is immobilized in a matrix (usually dextran) on the metal film [3]. Adsorption of a protein, antibody or antigen onto the bare metal film, followed by exposure of the biospecific surface to a bulk solution of analyte, is also used as an alternative method [4].

SPR-based sensors, including a dextran film for binding biospecific ligand, have so far been used for the kinetic analysis of monoclonal antibodies to whole virus particles [5]. Also, a streptavidin monolayer, immobilized onto a gold film containing biotin, is the basis for a specific sensor for the antigen sex hormone binding globulin. Both types of sensors afford low limits of detection.

In either case, periodic regeneration of the sensor surface, with cleaning and coating of the metal film, is needed. This technique, which requires no molecular label, has two main advantages, i.e., real time analysis and biospecific detection.

Small-sized molecules have been determined in different types of samples using an SPR-based sensor, for instance, in the monitoring of distilled products and alcohols [6]. Garcia-Ruiz et al. [6] used a thin layer of MgF_2 on a gold film to improve the mechanical properties and to ensure that the measurement range was adequate.

The scope of application of SPR sensors has recently been expanded by their use in immunoaffinity chromatography [7] of proteins, e.g. carboxymethylated dextran attached to a gold film provides a hydrophilic matrix onto which various macromolecules can be immobilized, thus, acting effectively like a chromatographic support.

The aim of this work was to characterize a detector prototype for high-performance liquid chromatography (HPLC), based on the SPR effect. Fine-tuning a new detector usually involves assessment of its repeatability, dynamic linear range and baseline noise and drift. In fact, band broadening vanes with the working conditions and so do the peak profiles. By investigating band broadening effects, one can abstract useful information on such detector features as the detector cell effective volume and the response time, as well as on their influence on the efficiency of the separation.

Therefore, it is necessary that a model is capable of explaining the shape of chromatographic peaks, which also enables the researcher to recognize the influence of such diverse factors as injection, connecting tubes, fittings, detector cell and response time on the peak profile [8]. The easiest way to do this is by assuming that the peaks fit an exponentially Gaussian function, since they are rendered asymmetric by band-broadening processes both inside and outside the column. While non-Gaussian peaks can be processed using statistical central moments, the procedure is prone to errors arising from baseline noise, data acquisition characteristics and baseline drift [9]. The exponentially modified Gaussian (EMG) method is an empirical one that uses graphically measured parameters to calculate central moments and miscellaneous chromatographic parameters.

The EMG function has been thoroughly reviewed [10] and evaluated [11] in order to determine the precision and accuracy of the equations derived for

such chromatographic figures of merit (CFOMs) as the decay constant, variance, statistical moments and skew and excess. It is a powerful tool as it allows non-ideal chromatographic peaks to be readily characterized from such graphical parameters as peak retention, height and width, which are best measured at 10% of the peak height.

Once the peak variance is calculated, the contribution made by each part of the chromatographic system can be evaluated, as the effects considered are independent of one another. Thus, the effective total variance [12] can be expressed as the sum of each variance.

The parameter, D, used to describe the injection profile and the flow-rate, provides information about the characteristics of the sample injection. For a rectangular injection profile with a time variance for the width equal to 0.607 times the peak height, D^2 is four; however based on the central moments method, D^2 is twelve. In contrast, for a purely Gaussian profile, the D^2 value is equal to 2π [13]. The greatest contribution to peak broadening arises from the chromatographic column, which reflects the influence of the number of plates which the column has. The actual efficiency is very difficult to determine accurately, due to errors made in calculating the number of plates from non-Gaussian peaks [14].

Finally, band broadening caused by the detector is due to the cell volume and the response time. Usually, the detector has the appropriate geometry and hydrodynamic conditions to function as a mixing chamber, which is unfavourable.

2. Experimental

2.1. Description of the SPR detector

The SPR detector was developed from the SPR sensor designed by Villuendas and Pelayo [15]. It consists of two parts, namely, the sensor head, where the SPR takes place, and the electronic unit, which includes a light-emitting diode (LED), the detector and the signal-processing module.

The light emerging from the LED through a multimode optical fibre (50 μm I.D.) reflects at an incidence angle of 67°, on one face of a BK7 glass prism, onto which a thin gold film (30 nm approximately) had been deposited previously. The choice of material to make the prism depends on the range of refractive indices that need to be detected. In our case, we detected changes from 1.33415 to 1.35580 RI units. As the material needed has to have a RI bigger than 1.35580 and be transparent to the light in the near infrared, BK7 glass with a refractive index of 1.51, was chosen. After the SPR is produced, the reflected light, the intensity of which depends on the RI of the effluent from the chromatographic column, is collected in the other optical fibre, to be read by the data acquisition unit. A scheme of this detector is shown in Fig. 1.

2.2. Chromatographic procedure

A 35 cm×4.5 mm I.D. Supelcosil LC–NH_2 alkylamine-bonded stationary phase column was used. The mobile phase consisted of acetonitrile–water (82:18, v/v) and was delivered at a flow-rate of 2 ml/min by an isocratic pumping system furnished with a pressure oscillation dampening device. The pump pressure ripple was below 0.5%. The injection system was a Rheodyne 7125 manual injection valve. The column temperature was kept at 30°C. A capillary tube (1 m×0.25 mm I.D.), covered with a thermal insulator, was used to connect the pump with a Hewlett-Packard HP1047A RI detector or with the SPR detector.

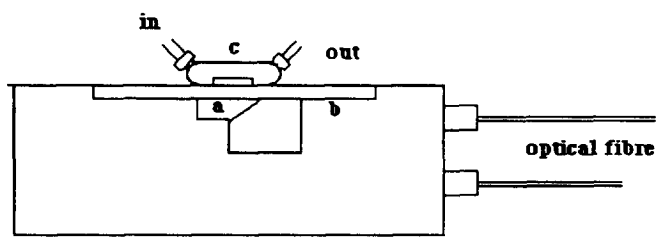

Fig. 1. Sensor head: a = BK7 prism, b = gold film, c = detector cell.

The optimum composition of the mobile phase was determined by a windows procedure [16].

3. Results and discussion

3.1. Optimization of the mobile phase composition

For efficient separation, the capacity coefficient of each compound must be known beforehand to calculate the bands. By choosing an appropriate resolution (e.g. 2.3), a critical band is then defined for every component using the following expression:

$$R_s = (\sqrt{N})/2 \cdot (K_j' - K_i')/(K_j' + K_i' + 2)$$

where K_j' and K_i' are the capacity coefficients for components i and j, respectively, and N is the number of theoretical plates. If any compound has a capacity coefficient lying in this band, the resolution is inadequate.

The influence of the mobile phase composition on the response of the SPR detector is the same as that of the RI detector, since both of them are based on the same physical property, i.e., RI. For instance, changes in the composition of the mobile phase during the chromatographic process result in changes in the RI, which produce baseline drift. For this reason, care was taken to avoid variation in the mobile phase composition from experiment to experiment, as well as during the chromatographic procedure. All of the mixtures were prepared using volumetric flasks and calibrated glassware. In between runs, the column was washed for 30 min at a flow-rate of 2 ml/min.

Acetonitrile–water mixtures with more than 80.5% acetonitrile were found to result in no overlapping of bands and hence provided optimal conditions. A ratio of 82:18 (v/v) was finally used, to ensure good resolution (2.3) and a short chromatographic run-time (15 min).

3.2. Influence of the wavelength of the LED

Two wavelengths were tested, 1300 and 850 nm. Lower noise was expected for an 850-nm LED than for a 1300-nm LED. In Fig. 2, the evolution of noise with time can be seen and can be compared to that

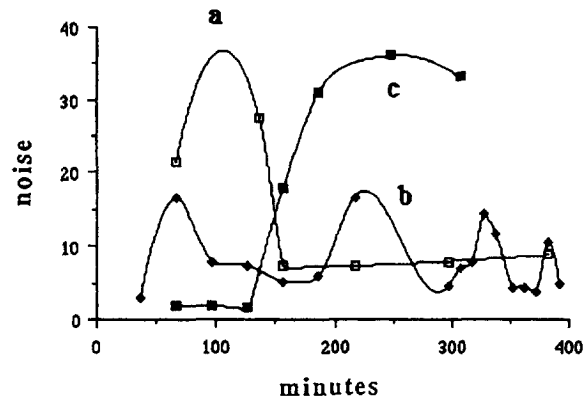

Fig. 2. Temporal noise evolution for the 850 nm (a) and the 1300 nm (b) SPR, each furnished with a system to correct the effect of temperature on the light emission of the LED and connected ends and for the RI detector (c) (noise ×100). Supelcosil LC–NH_2 column; mobile phase, acetonitrile–water (82:18, v/v); flow-rate, 2 ml/min; volume of injection, 20 μl.

obtained with the RI detector. It is also shown that stabilization of the SPR detector that was furnished with the 1300-nm LED occurred 50 min before that of the RI detector.

Sensitivity was also found to be dependent on the wavelength used. If the field distribution of the surface plasmon is studied with regards to the perturbation theory, it is found that the minimum variation in RI that can be detected is inversely proportional to the wavelength used and to the square root of the absolute value of the real part of the dielectric constant of the metal [20] (gold in our case). That is to say, if the surface plasmon suffers a strong attenuation due to light absorption in the metal, then its intensity decays exponentially with an attenuation constant that is inversely proportional to the wavelength used. Since the metal remains the same, the only way to affect the sensitivity is to change the wavelength of the light used. As expected, the shorter the wavelength was, the lower the sensitivity obtained was. The more sensitive the device is, the more it is affected by changes in temperature and mobile phase composition.

This noise effect was evaluated at the highest and lowest amplification power. For this purpose, the sucrose peak height-to-noise ratio was calculated for the RI and SPR detectors, using the two above-

Table 1
Influence of the wavelength of the LED

Detector	Amplification power	*H*:noise ratio	Sucrose (μg)
RI	$0.31 \cdot 10^{-5}$	795	81
	$32 \cdot 10^{-5}$	1378	81
SPR (850 nm)	128	6	139
(no fixed, Peltier)	64	7	139
SPR (1300 nm)	32	4	133
(no fixed, Peltier)	8	10	133

RI units: refractive index units. SPR: a factor related to the amplification power; *H*:noise represents the peak height-to-noise ratio. Peaks were obtained under optimum conditions: Supelcosil LC–NH_2 column; mobile phase, acetonitrile–water (82:18, v/v); flow-rate, 2 ml/min; volume of injection, 20 μl.

mentioned wavelengths. The results are shown in Table 1.

Increasing the signal amplification power had little effect on the signal-to-noise ratio when using an 850-nm LED, due to its lack of sensitivity, but the effect was greater for the 1300 nm LED. This behaviour is similar for the RI detector.

Repeatability was tested by performing sucrose injections. Fructose and glucose were discarded for this purpose, due to their reducing properties, they reacted with the alkylamine stationary phase to yield Schiff bases.

After a stabilization period (see Table 2), eight injections of sucrose were carried out. The relative standard deviations (R.S.D.s) of the peak areas thus obtained, as well as the time required to stabilize each detector, are shown in Table 2 for two different LED wavelengths and for the RI detector. It should be noted that the RI detector and the SPR detector with the 1300 nm LED provided good repeatability and faster stabilization times.

Table 2
Repeatability

Detector	Time (min)	R.S.D. (%)	Injection (μg)
RI	150	0.41	274
SPR (850 nm)	150	23.2	138
SPR (1300 nm)	100	1.3	133

Injected sugar, sucrose. Supelcosil LC–NH_2 column; mobile phase, acetonitrile–water (82:18, v/v); flow-rate, 2 ml/min; volume of injection, 20 μl.

3.3. Influence of the connection between the sensor head and the optical fibre and thermostabilization of the LED emission

Two kinds of connections were tested:

- Optical welder, fixed connection.
- Connectorized ends, easy disconnection.

Movement of the fibres is one source of noise that can be diminished by using a multimode optical fibre. Then the connections between the end of the fibre and the sensor head are the main source of noise in the optical part of the instrument.

An optical welder has a fixed connection and eliminates this contribution, however, this design makes it difficult to move the instrument.

Temperature changes affect the signal in two different ways, i.e., by affecting the RI and the properties and performance of the optics. In traditional RI detectors, the optic part of the device is fixed on a solid base and isolated from its surroundings, to avoid such things as shaking, light scattering, focussing of the lenses and mirrors due to the changes of temperature, etc. In our design, the main influence on the system is caused by temperature variations on the LED, emissions from which are strongly affected by temperature. In order to simplify the design, electronic thermal stabilization of the LED was avoided, but turned out to be necessary, as low noise levels and a driftless baseline are desirable. For this reason, the detector was furnished with a Peltier system.

When the Peltier system was avoided, cyclic baseline drift, dependent on the natural evolution of temperature, was observed. To verify this assertion, the sensor head (where the SPR effect takes place) was replaced with an optical attenuator that diminished the light intensity provided by the 1300-nm LED in a manner similar to that of the surface plasmon. This cyclic drift (over a period of 24 h) is clearly shown in Fig. 3, where the curves obtained for two consecutive 24-h experiments are shown.

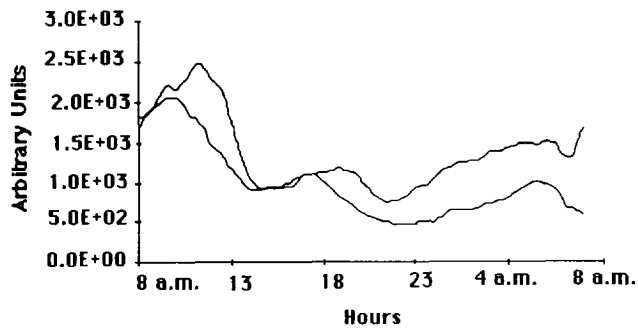

Fig. 3. Baseline drift caused by the electronic part of the SPR detector. The sensor head was replaced with an attenuator that behaves as a surface plasmon.

3.4. Dynamic linear range (DLR)

The DLR for the SPR and RI detectors was determined as the range between the limit of detection (LOD) and the upper limit of linearity (ULL). Clayton et al. [17] defines the LOD in such a way that protection against false positives and negatives is assured. In order to calculate the ULL [18], calibration data were fitted to a second order polynomial curve, which was then first derivatized, dx/dy being equal to zero and x being solved. Table 3 shows the LOD and ULL values obtained.

The linear calibration model was used in all instances. The regression coefficient obtained was greater than 0.990 for both detectors.

The RI detector provided slightly better LODs than the SPR one, mainly due to differences in the broadening of peaks, which were larger for SPR. For the SPR detector, the wavelength used had a decisive influence in lowering the LOD, i.e. the shorter the wavelength, the higher the LOD.

It was impossible to calculate the DLR for glucose and sucrose using the 850-nm LED, since the sensitivity was very poor and imprecision in the calculated area was noticed.

The broad DLR corresponds to the result obtained using the SPR detector, which was almost three-times broader than that calculated for the RI detector.

Fig. 4 shows a chromatogram obtained with the SPR detector (1300 nm, connected ends and thermal stabilization system) and Fig. 5 shows a chromatogram obtained with the RI detector. As can be seen,

Table 3
Dynamic linear range

Detector	Fructose		Glucose		Fructose	
	LOD (μg)	ULL (μg)	LOD (μg)	ULL (μg)	LOD (μg)	ULL (μg)
RI	6	722	7	248	13	342
SPR (1300 nm) no fixed, no Peltier	41	418	70	387	69	168
SPR (1300 nm) fixed, Peltier	4	885	16	154	33	151
SPR (850 nm) no fixed, Peltier	83	177	–	–	–	–
SPR (1300 nm) no fixed, Peltier	5	94	13	170	22	354

Supelcosil LC–NH_2 column: mobile phase, acetonitrile–water (82:18, v/v); flow-rate, 2 ml/min; volume of injection, 20 μl.

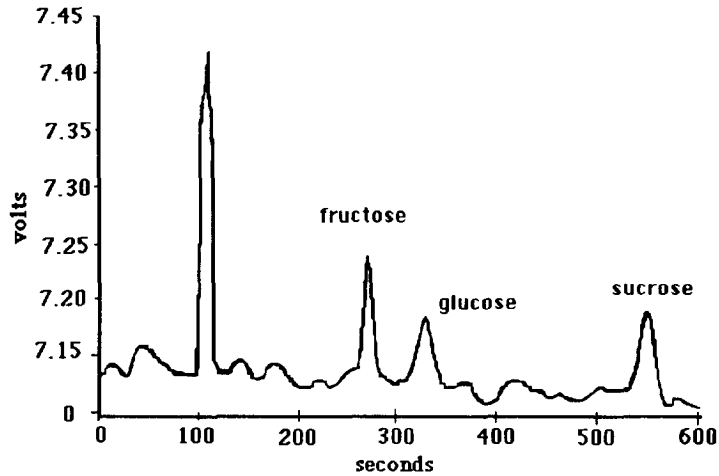

Fig. 4. Chromatogram obtained with the SPR detector for 100 μg of fructose, 100 μg of glucose and 125 μg of sucrose. Supelcosil LC–NH_2 column; mobile phase, acetonitrile–water (82:18, v/v); flow-rate, 2 ml/min; volume of injection, 20 μl.

the baseline was quite smooth and stable for the SPR detector.

3.5. Extra-column band broadening

The different sources of band broadening, injection, capillary tubing, detector and column, can be dealt with individually and then be summed quadratically through their variances. In this study, no column switching was performed and the observed variance was:

$$s^2_{\text{total}} = s^2_{\text{injection}} + s^2_{\text{tube}} + s^2_{\text{detector}}$$

Since the capillary tubing used in this experiment was the same for both detectors, as was the injection system, the differences essentially arose from the contributions of the detectors to band broadening.

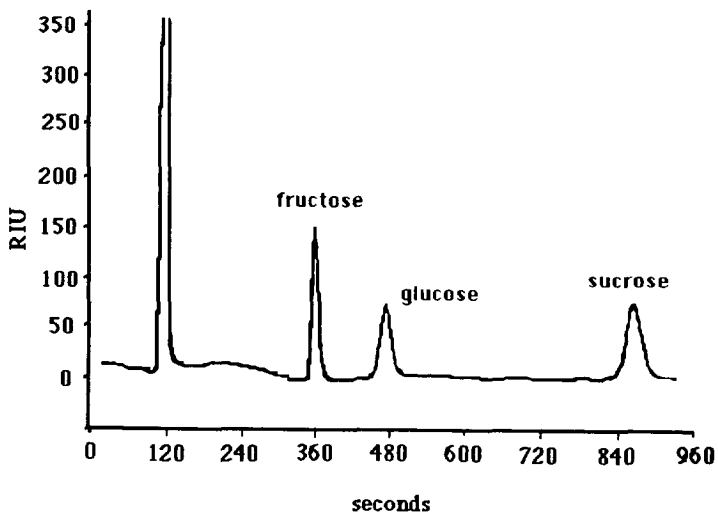

Fig. 5. Chromatogram obtained with the RI detector for 100 μg of fructose, 100 μg of glucose and 125 μg of sucrose. Supelcosil LC–NH_2 column; mobile phase, acetonitrile–water (82:18, v/v); flow-rate, 2 ml/min; volume of injection, 20 μl.

The potential effect of the injection was studied for the sake of completeness.

For this purpose, the flow-rate was kept constant (at 2 ml/min) and the injected volume was varied from 5 to 50 μl (100 μg of sucrose were injected in each experiment). A plot of calculated s^2 vs. V_{inj} provided a second order polynomial curve and the second order coefficient reflects the influence of the injection. The adjusted polynomial curves for the RI and SPR detectors were:

$$s^2_{RI} = 0.0001 + 0.0017V_{inj} + 0.0375V^2_{inj}$$

$$s_{SPR} = 0.0001 + 0.0002V_{inj} + 0.0375V^2_{inj}$$

Both detectors are affected in the same way by the injection. The calculated value for D^2 was 6.73 for the former and 6.67 for the latter, therefore, a Gaussian profile was assumed for both cases.

The first order coefficient told us that the additional band broadening resulting from the effects of instrumental broadening and the plug injection band was more influential for the RI detector than for the SPR detector.

The independent term denoted the total variance at zero injected volume, which was the same in both cases.

This experiment was also carried out by switching the chromatographic columns and then treating the variance of the resulting peaks in the same way.

$$s^2_{RI} = 0.0027 + 0.0101V_{inj} + 0.0381V^2_{inj}$$

$$s^2_{SPR} = 0.0036 + 0.0119V_{inj} + 0.0395V^2_{inj}$$

D^2 was also calculated from these equations and was found to be in good agreement with the previously calculated value, 6.56, for the RI detector and 6.41 for the SPR detector.

In order to determine the influence of the detector, the injected volume (containing 100 μg of sucrose) was kept constant and the flow-rate was varied from 0.5 to 2.5 μl/min. A plot of s^2 vs. F was performed and fitted to a second order polynomial curve:

$$s^2_{RI} = 0.0001 + 0.0003\ 1/F + 0.0010\ 1/F^2$$

$$s^2_{SPR} = 0.0002 + 0.0001\ 1/F + 0.0010\ 1/F^2$$

Once D^2 was known, the apparent cell detector volume for the RI and SPR detectors was calculated. This turned out to be 31 μl in both cases. This apparent volume is three times the usual detector volume in HPLC. The manufacturer's nominal value was 14 μl for the RI detector and 10 μl for the SPR one. The difference can be related to the contribution of the cell detector connections in the SPR detector and the thermostability system located before the detection cell in the RI one, which contribute 78.5 μl to the dead volume.

If the detectors are treated as mixing chambers, the response times can be calculated easily and were found to be 0.93 s for both detectors, and were quite acceptable.

3.6. Efficiency loss

We used relative plate loss (RPL) to quantify the contributions of symmetric and asymmetric band broadening to the overall band broadening.

$$\mathrm{RPL} = (t_g/t_r)^2 \cdot (N_g - N_s)/N_g$$

where N_g is the maximum possible efficiency that can be achieved if the chromatographic separation provides symmetric peaks, which always exceeds the actual value because of various processes taking place in the column; t_g is the retention time for the peak when no distortion occurs and t_r is the real retention time. N_s is the observed efficiency, calculated using an empirical equation based on the exponentially modified Gaussian function to describe the peaks.

The loss of efficiency was found to be less for the RI detector (4.1%) than for the SPR detector (11.1%), due to its broader peak profile, mainly resulting from capillary tubes and the detector cell connections. In addition, the broader peak profile obtained with the SPR detector affected the LOD, since, the broader a peak was, the more difficult it was to determine its beginning and end, resulting in difficulty in calculating the area. However, the differences in band broadening between the detectors were not very large (0.63 min for the SPR and 0.56 min for the RI, measured at 10% of the peak height), which is why their LOD values were quite similar.

4. Conclusions

The SPR detector offers several advantages over the RI detector, namely:

1. Shorter baseline stabilization time; 50 min less than the RI detector.
2. Compact design.
3. Easy operation.
4. The use of fibre optics reduces the noise by suppressing light scattering.
5. Lower cost.

In contrast, the SPR detector has a narrower DLR and is more strongly affected by extra-column band broadening, its relative plate loss being twice that for the RI detector. The source of this extra-column band broadening was the design of the detector cell. A good improvement in suppressing the influence of the surroundings on the detector was achieved due to suppression of light scattering by using a multimode optical fiber, which also made the detector easy to transport. The optical design reduces the influence of temperature, as shown by the experiments carried out with and without the temperature stabilization system for the LED.

Further work on this subject has to focus on the elimination of all sources of extra-column band broadening, by improving the design of the detector cell, as well as that of the connections. We also have to develop more applications for our detector and compare the results obtained with those of several universal detectors, if they are available.

References

[1] S.A. Wilson and E.S. Yeung, Anal. Chem., 57 (1985) 2611.
[2] H. Roether, Surface Plasmons on Smooth and Rough Faces and Gratings, Springer, Berlin, 1982.
[3] B. Johnsson, S. Lofas and G. Linquist, Anal. Biochem., 198 (1991) 268.
[4] H. Morgan and D.M. Taylor, Biosensor and Bioelectronics, 7 (1992) 405.
[5] M.C. Dubs, D. Altschub and M.H.V. Van Regenmortal, J. Chromatogr., 597 (1992) 391.
[6] E. Garcia-Ruiz, I. Garces, C. Aldea, M.A. Lopez, J. Mateo, J. Alonso-Chamarro and S. Alegret, Sensors Actuators, 27 37–38 (1993) 221.
[7] M. Brighamburke and S.I. Oshannessy, Chromatographia, 35 (1993) 49.
[8] S. Martin, C. Eon and G. Guiochon, J. Chromatogr., 180 (1975) 229.
[9] F. Dondi, A. Betti and C. Bighi, Anal. Chem., 53 (1981) 496.
[10] M.S. Jeansome and J.P. Foley, J. Chromatogr. Sci., 29 (1991) 258.
[11] M.S. Jeansome and J.P. Foley, J. Chromatogr., 594 (1992) 1.
[12] J. Sternberg, Advances in Chromatography, Marcel Dekker, New York, 1966.
[13] H.H. Lauer and G.P. Rozing, Chromatographia, 14 (1981) 641.
[14] J.J. Kirkland, W.W. Yau, H.J. Stoklosa and C.H. Dilks, J. Chromatogr. Sci., 15 (1977) 303.
[15] F. Villuendas and J. Pelayo, Sensors Actuators A, 25–27 (1991) 449.
[16] H. Colin, A. Krstulovic, G. Guiochon and J.P. Bounine, Chromatographia, 17 (1983) 209.
[17] C.A. Clayton, J.W. Hines and P.D. Elkins, Anal. Chem., 59 (1987) 2506.
[18] P.L. Bonate, J. Chromatogr. Sci., 28 (1990) 559.
[19] J.W. Sadowski J. Lekkala and I. Vikholm, Biosensors Bioelectronics, 6 (1991) 439.
[20] W. Lukosz, Biosensors Bioelectronics, 6 (1991) 215.